

RESEARCH

Open Access



Structure-guided engineering of α -ketoisocaproate dioxygenase increases isobutene production in *Synechocystis* sp. PCC 6803

Conrad Schumann^{1†}, Amit Kugler^{1†}, Bhavik Ashwin Shah¹, Gustav Berggren¹, Henrik Land¹, Cecilia Blikstad¹ and Karin Stensjö^{1*}

Abstract

Isobutene is a promising precursor for jet fuel due to its high energy density and favorable combustion properties. Light-driven bioproduction of isobutene has recently been investigated as an alternative strategy to crude oil refinement or fermentation-based manufacturing processes by harnessing the unicellular cyanobacterium *Synechocystis* sp. PCC 6803 and the α -ketoisocaproate dioxygenase (*RnKICD*) from *Rattus norvegicus*. However, the obtained production level was not sufficient, partially due to the promiscuous activity of *RnKICD*. The enzyme catalyzes both the reaction with *p*-hydroxyphenylpyruvate (HPP) for homogentisate formation, as well as the reaction with α -ketoisocaproate (KIC), the precursor for isobutene synthesis. Here, to overcome this bottleneck step in the isobutene biosynthesis, protein engineering was employed to improve *RnKICD* activity and in vivo isobutene production. Purified *RnKICD* variants were characterized by measuring in vitro KIC and HPP consumption rates, as well as isobutene formation rate. The active site mutations F336V, N363A altered the KIC and HPP consumption rates, while the KIC-to-isobutene conversion ratio was only marginally affected. Besides, the *RnKICD* variants F336V, N363A and F336V/N363A exhibited a substantially enhanced substrate selectivity for KIC over HPP. Among the examined engineered *Synechocystis* strains, Syn-F336V showed a 4-fold improvement in isobutene production, compared to the base strain (Syn-*RnKICD*). Our findings reveal that residues F336 and N363 play a crucial role in substrate interactions, as targeted mutations at these sites shifted the substrate selectivity towards KIC while F336V elevated the in vivo isobutene production levels significantly. We conclude that engineering the active site of *RnKICD* is a potent tool for improving isobutene bioproduction in *Synechocystis*.

Highlights

1. Promiscuous α -ketoisocaproate dioxygenase (KICD) from *Rattus norvegicus* was overproduced in *Synechocystis* sp. PCC 6803.
2. Protein engineering was used to improve substrate selectivity.
3. The generated F336V variant led to a 4-fold increase in isobutene production in vivo.

[†]Conrad Schumann and Amit Kugler have contributed equally.

*Correspondence:
Karin Stensjö
karin.stensjo@kemi.uu.se



Keywords Protein engineering, Cyanobacteria, Isobutene, Alkenes

Introduction

Isobutene is a volatile C₄-alkene, serving as platform molecule for synthesizing numerous industrial products, such as butyl rubber, terephthalic acid, specialty chemicals and a gasoline performance additive [17]. In addition, isobutene can be used as precursor for the manufacturing of jet-fuels, for which isobutene undergoes oligomerization and hydrogenation reactions [19]. At present, isobutene is primarily produced by extraction from steam cracking of petroleum hydrocarbons [8].

Biofuel manufacturing by microorganisms offers a promising approach to support a circular bioeconomy. The environmental impact of a production can be reduced by recovering the remaining value of by-products or waste, e.g. using captured CO₂ in the production of valuable compounds like isobutene [30]. As a volatile gas, isobutene can be efficiently collected and purified from off-gas, minimizing downstream processing costs and risk of in vivo accumulation of the fuel compound to a toxic level.

We have recently described the light-driven biosynthesis of isobutene from CO₂ in the model cyanobacterium *Synechocystis* sp. PCC 6803 (hereafter *Synechocystis*) [18]. This was achieved by metabolic engineering through heterologous expression of the gene encoding α -ketoisocaproate dioxygenase from *Rattus norvegicus* (*RnKICD*; EC 1.13.11.27). However, the low isobutene yields make this system economically less feasible compared to fermentative processes that use sugars as feedstocks [7, 32] and limits its application/operation at an industrial scale [18].

Several reported enzymes involved in biocatalytic production of isobutene catalyze the irreversible decarboxylation of a C₅ branched chain carboxylic acid [5, 7, 23]. The catalyzed reaction is either facilitated via oxidative, ATP-dependent [7, 23] or redox active cofactor dependent decarboxylation [5, 24]. The mononuclear Fe(II)-dependent *RnKICD* has been reported to catalyze the conversion of α -ketoisocaproate (KIC) and molecular oxygen into 3-hydroxy-3-methylbutyrate (HMB) [25, 26] followed by a non-enzymatic decomposition reaction to yield isobutene [23]. In our previous study, we found that in vitro isobutene production rate was higher than the isobutene formation rate resulting from spontaneous HMB decomposition. This demonstrates that isobutene can be directly converted from the C₆ branched chain

carboxylic acid KIC by undergoing two decarboxylation steps [18]. Hence, *RnKICD*'s promiscuous nature of converting KIC results either in the formation of HMB or isobutene, with low product specificity for isobutene. However, the mechanism underlying the isobutene formation remains unclear.

RnKICD shares a 100% amino acid sequence identity with the rat ρ -hydroxyphenylpyruvate dioxygenase (HPPD) which converts ρ -hydroxyphenylpyruvate (HPP) into homogentisate (HGA) [1, 25, 26]). Thus, mammalian HPPD and KICD is the same enzyme that displays substrate promiscuity towards a variety of α -keto acids [4]. In plants, HGA acts as a precursor for plastoquinone-9 and α -tocopherol synthesis, which are important for the photosynthesis process and plant survival [20]. Due to the essential physiological function of HPPD, this enzyme has been intensively investigated as a target for herbicide discovery [33].

Protein engineering is an important part of metabolic engineering which involves amino acid substitutions for developing enzymes with increased catalytic rate, substrate specificity or stability [2]. In turn, such modifications can enhance titers and yields of the compound of interest [11]. Protein engineering strategies include directed evolution (random mutagenesis), rational design (site-directed mutagenesis), or a combination of both (semi-rational) [36]. The choice of approach depends on existing knowledge of the enzyme being studied and the availability of screening or selection methods for the variants produced. Recent crystallographic data has identified key residues within the HPPD binding pocket, involved in substrate (HPP) binding and catalytic efficiency [10], which can assist in repurposing HPPD activity by rational and semi-rational designs.

In this study, we generated *RnKICD* variants with active site amino acid substitutions based on rational and semi-rational protein design. We aimed to increase selectivity towards KIC (as the isobutene precursor), and ultimately enhance the isobutene production from cultivated *Synechocystis*. All engineered *RnKICD* enzyme variants displayed lowered in vitro consumption rates for the two substrates HPP and KIC, while the apparent selectivity towards KIC was increased. The generated strain SynF336V overexpressing *RnKICD*-F336V showed a 4-fold higher isobutene titer, compared with the base strain. Our results demonstrate that protein engineering of *RnKICD* is a feasible strategy to significantly increase the

production of isobutene synthesized by metabolically-engineered *Synechocystis*.

Methods

Bacterial strains and growth conditions

E. coli TOP10 (Invitrogen) were used for cloning, conjugation and screening for site-directed mutants, as well as assessing the plasmid mutant library quality. *E. coli* BL21 (DE3) was used for the heterologous overexpression of the generated RnKICD mutants. *E. coli* TOP10 cells were cultivated in lysogeny broth (LB) medium (Sigma Aldrich) or on 1.5% agar (w/v) plates, at 37 °C. *E. coli* BL21 (DE3) cells were cultivated in Terrific Broth (TB) medium (Sigma Aldrich), at 37 °C. All medium were supplemented with (50 µg mL⁻¹ kanamycin).

The glucose-tolerant *Synechocystis* sp. PCC 6803 sub-strain [31] was used throughout the study. *Synechocystis* cells were cultivated in BG11 [29] medium, or on 1.5% agar (w/v) plates, under 15 µmol photons m⁻² s⁻¹ at 30 °C or stated otherwise. All *Synechocystis* strains harboring the pEEK2-Km^R vector with or without KICD variants were supplemented with 50 µg mL⁻¹ kanamycin. All strains used in this study are listed in Table 1.

Homology modeling and molecular docking

To obtain structural models of both the open and the closed conformation of RnKICD homology modeling

was used. More specifically, a homology model in the open conformation was made using AtHPPD (PDB ID: 5XGK) as template and a homology model in the closed conformation was made using HsHPPD (PDB ID: 3ISQ) as template using YASARA [13] structure version 18.3.23 following previously described protocols [14]. Any ligands were removed from the resulting models and energy minimization was performed inside a water-filled simulation cell (cuboid shape, 5 Å around all atoms) with periodic boundaries using the AMBER 14 force field [3]. The energy minimized models were then subjected to docking simulations as previously described [14] using both HPP and KIC as ligands (50 docking runs per model/substrate combination). The most prevalent docking conformation out of the 50 runs for each docking simulation was chosen as the representative for further analysis.

Bioinformatic analysis

In order to obtain a representative collection of sequences for bioinformatic analysis, separate BLASTp searches were performed using template sequences from different branches of life: *Rattus norvegicus* (Genbank ID: NP_058929.1), *Arabidopsis thaliana* (Genbank ID: NP_172144.3) and *Pseudomonas fluorescens* (Genbank ID: 1CJX_A). 2839 sequences were combined and trimmed to 262 sequences by removing 90% redundancy

Table 1 Strains and genetic constructs used in this study

Strain	Construct	Description	References
Syn-EVC	pEEK2-Km ^R	<i>Synechocystis</i> sp. PCC 6803 strain harboring pEEK2 plasmid for Km resistance as empty vector control	Mustila et al. (2021)
Syn-RnKICD	pEEK2-RnKICD	<i>Synechocystis</i> sp. PCC 6803 strain harboring pEEK2 plasmid for Km resistance and RnKICD	Mustila et al. (2021)
Syn-N363A	pEEK2-N363A	<i>Synechocystis</i> sp. PCC 6803 strain harboring pEEK2 plasmid for Km resistance and N363A mutation in RnKICD	This study
Syn-F336V	pEEK2-F336V	<i>Synechocystis</i> sp. PCC 6803 strain harboring pEEK2 plasmid for Km resistance and F336V mutation in RnKICD	This study
Syn-F336V/N363A	pEEK2-F336V/N363A	<i>Synechocystis</i> sp. PCC 6803 strain harboring pEEK2 plasmid for Km resistance and F336V/N363A mutation in RnKICD	This study
EcBL21-EVC	pETBB-Km ^R	<i>E. coli</i> BL21(DE3) strain harboring pETBB plasmid for Km resistance as empty vector control	Mustila et al. (2021)
EcBL21-RnKICD	pETBB-RnKICD	<i>E. coli</i> BL21(DE3) strain harboring pETBB plasmid for Km resistance and RnKICD	Mustila et al. (2021)
EcBL21-Q251E	pETBB-Q251E	<i>E. coli</i> BL21(DE3) strain harboring pETBB plasmid for Km resistance and Q251E mutation in RnKICD	This study
EcBL21-Q265E	pETBB-Q265E	<i>E. coli</i> BL21(DE3) strain harboring pETBB plasmid for Km resistance and Q265E mutation in RnKICD	This study
EcBL21-N363A	pETBB-N363A	<i>E. coli</i> BL21(DE3) strain harboring pETBB plasmid for Km resistance and N363A mutation in RnKICD	This study
EcBL21-F336V	pETBB-F336V	<i>E. coli</i> BL21(DE3) strain harboring pETBB plasmid for Km resistance and F336V mutation in RnKICD	This study
EcBL21-F336V/N363A	pETBB-F336V/N363A	<i>E. coli</i> BL21(DE3) strain harboring pETBB plasmid for Km resistance and F336V/N363A mutation in RnKICD	This study

using Jalview (version 2.11.3.3). A multiple sequence alignment was then performed using ClustalΩ. [28].

Plasmid construction

The plasmids used in this study are detailed in Table 1. For heterologous expression in *E. coli* BL21 (DE3), previously constructed pETBB-Km^R, and pETBB-*RnKICD* plasmids were used [18]. The self-replicating plasmids pEEK2-Km^R and pEEK2 were used for expression in *Synechocystis*. pEEK2-*RnKICD* was previously constructed and contains the strong constitutive promoter *Ptrc-core* and a codon optimized *RnKICD* gene [18]. Selected mutations were introduced into the *RnKICD* gene on pETBB-Km^R, and pEEK2-Km^R. All primers used for site directed mutagenesis are listed (Additional file 1: Table S1). The coding sequence for Strep-tagged WT *RnKICD* is listed as well (Additional file 1).

All primers were synthesized and supplied by IDT (USA). The site-directed mutagenesis was carried out by an overlapping PCR-based method [37]. The entire plasmids were amplified using Phusion Hot Start II High-Fidelity DNA Polymerase (Thermo Fisher Scientific), with subsequent digestion with DpnI enzyme [27]. The PCR products were then used for conjugation of *Synechocystis*.

Site-saturation mutagenesis

The pETBB-*RnKICD* plasmid [18] was used as the initial template for site-saturation mutagenesis and for the generation of two plasmid libraries with mutations in the positions Q334 and F336. For each mutant library four 5'-phosphorylated primers were designed and ordered by IDT (USA) (Additional file 1: Table S2). Mutations were introduced by miss-matches in the 5'-end of the primers, with degenerate primers allowing for various codons in one reaction [34]. Using a primer mix with two degenerate (NDT and VHG) codons and one defined codon (TGG) limited introduced codons to 22 covering all 20 proteinogenic amino acid and excluding stop codons [12] This approach reduced genetic diversity, thus lowering the screening effort required. For the F336 library, forward primers contained the mutational codons, while reverse primers for the Q334 library comprised the mutational codons as a reverse complement. The NDT:VHG:TGG primers for both libraries were mixed at 12:9:1 ratio [12] and used as forward and reverse primers in the PCR for F336 and Q334 mutant library, respectively. The T_m for all eight primers ranged between 62 and 65 °C (NEB T_m calculator, 2022).

Site-saturation mutagenesis used pETBB-*RnKICD*_NStrepII (6.4 kb) as the template in eight 20 µL inverse PCRs [21]. For details, see Additional file 1: Table S2. Due to the variety of primers an annealing temperature gradient was applied to counteract preferential annealing. PCR products were gel purified, then incubated for 15 min at 37 °C with DpnI fast digest (Thermo Fischer) to remove template DNA, cleaned with a PCR clean-up kit (Zymo Research) and ligated overnight with Quick Ligase (New England Biolabs at room temperature (RT)). The ligation mix was used directly to transform *E. coli* TOP10 and *E. coli* BL21 (DE3) cells. Approximately 500 clones from each mutant library were pooled sequenced to evaluate the library quality based on introduced codons and the nucleobase distribution. This quick quality control (QQC) of the libraries confirmed effective template DNA removal and intended codon diversity, with mutations validated by Sanger sequencing (Mix2Seq, Eurofins Genomics).

Protein production and purification

All *E. coli* culturing was done in terrific broth (TB) medium with kanamycin (50 µg mL⁻¹). *E. coli* BL21 (DE3) cells (Invitrogen), harboring pETBB-*RnKICD* plasmids were cultured overnight in 20 mL medium in 100 mL Erlenmeyer flasks, at 37 °C and 190 rpm. The culture was then diluted to OD_{600nm} 0.1 and incubated in 1 L in a 3 L Erlenmeyer flask, at 37 °C and 190 rpm. Upon reaching OD_{600nm} 0.6–0.8, the gene expression was induced with 0.5 mM IPTG, the temperature lowered to 20 °C, and incubation continued for 20 h. Cells were harvested by centrifugation (Sorvall RC-3B Plus, GMI) at 4 °C, 7277g for 10 min and stored in –80 °C. Cells were lysed by resuspending in 50 mM HEPES (pH 7.5) with 1.2 mg mL⁻¹ lysozyme, 0.06 mg mL⁻¹ each of DNase, RNase, MgCl₂ (2.4 mg mL⁻¹), and EDTA free cComplete™ protease inhibitor (Roche). After 30 min incubation, the suspension was sonicated on ice (Sonic Vibra Cell, CV33 tip) for 1 min at amplitude 50% (10 s on and 20 s off). Soluble proteins were separated by ultracentrifuge (Culter Optima L-90K, rotor 70Ti, Beckman) (40 min, 4 °C, 257,000g, and filtrated through a 0.22 µm filter (Sigma-Aldrich)).

Proteins were purified at 4 °C using an ÄKTA pure FPLC system with two tandem Strep-Tactin Sepharose columns (StrepTrap HP 5 mL, Cytiva), with minor modifications to the manufacturer's protocol using 50 mM HEPES (pH 7.5) as binding and 2.5 mM D-desthiobiotin in 50 mM HEPES (pH 7.5) as elution buffer. Purified proteins were concentrated with 30 kDa cut-off filters (Amicon, Merck Millipore) at 4 °C, 4500g for 40 min. Protein purity was assessed by SDS-PAGE, and concentration was

determined at 280 nm using a NanoDrop (Thermo Fisher) with and Molar extinction coefficient of $55,600 \text{ M cm}^{-1}$ (ProtParam tool on the ExPASy Server, [6]).

Conjugation of *Synechocystis* sp. PCC 6803

Synechocystis was conjugated by Triparental mating (Elhai et al. 1997). *E. coli* TOP10 cargo cells (carrying pEEK2 plasmids) and *E. coli* HB101 helper cells (carrying pRL443-AmpR conjugative plasmid) were cultivated overnight in LB medium with $50 \mu\text{g mL}^{-1}$ kanamycin at 37°C . Cells were collected by centrifugation and resuspended in fresh liquid LB medium without antibiotics. Then, a mixture of wildtype *Synechocystis* (200 μl), cargo cells (1 ml) and helper cells (1 ml), was incubated under $30 \mu\text{mol photons m}^{-2} \text{ s}^{-1}$ at 30°C for 2 h. The mixture was then spread on a filter (GN-6 Metrical, Pall Lab) placed on a BG11 agar plate without antibiotics for 24 h of incubation at 30°C . Individual colonies (Table 1) were selected by transferring the filter onto BG11 agar plates with $50 \mu\text{g mL}^{-1}$ kanamycin and assessed by PCR using gene-specific primers (Additional file 1: Table S1).

Substrate consumption assay using 2,4-dinitrophenylhydrazine (DNPH)

An assay for determining KICD activity, based on a previously described method Gong et al. [9], was adapted for KIC and HPP consumption measurements. For the assay calibration, HPP and KIC concentration standards in the range from 0.1 to 3 mM were prepared in the reaction buffer (10 mM MES, 150 mM NaCl, pH 6.0) with 0.5 mM FeSO_4 , 0.5 mM sodium ascorbate, and 1 mM dithiothreitol and measured as triplicates. A blank was prepared from the same buffer that did not contain any substrate. The 2,4-dinitrophenylhydrazine (DNPH) assay was started by adding 25 μL of a calibration standard or library screening sample to 25 μL DNPH ethanol solution to a well in a microplate. By contrast, the samples from the activity measurements were mixed in a ratio of 1:1 with the DNPH reagent in a reaction tube. Thereafter, 50 μL of the mixture was added to a well in a microplate. The 96-well plates were then incubated for 40 min at 30°C which allowed the derivatization of KIC and HPP with DNPH. Next, 200 μL 1M NaOH ethanol solution were added to each well. After another 15 min of incubation at 30°C , the absorbance at 540 nm was measured in a plate reader (Hidex).

Assessment of substrate consumption

In vitro activity of all purified KICD variants was measured by determining the KIC and HPP depletion over time using an endpoint assay. Each in vitro reaction contained 4.2 μM enzyme, 2.5 mM of either HPP or KIC in the reaction buffer (10 mM MES, 150 mM NaCl, pH 6.0) with 0.5 mM FeSO_4 , 0.5 mM sodium ascorbate, and 1 mM dithiothreitol. Prior to the start of the reaction the enzymes were incubated at 30°C for 10 min in the reaction buffer. For the whole experiment, the enzymatic reaction was incubated in a heat block at 30°C . The reactions were sampled and stopped by mixing them with the acidic 95% ethanol DNPH solution resulting in enzyme denaturation. Triplicate enzymatic reactions were run in parallel and sampled at different time points between 0 and 90 min. Additionally, a negative control (NC) reaction without enzyme and a blank without substrate were prepared and sampled after 0, 30, and 60 minutes. The samples from the reaction replicates were pooled in one mixture with DNPH solution for each timepoint so that it contained equal volumes of reaction sample and DNPH solution. After the sample collection was finished, 50 μL of each sample were separately applied to three wells of a microplate. These technical replicates of the DNPH assay measurements were used to determine an average values standard deviation.

Cultivation and screening of site specific saturation-mutagenesis libraries

After transformation with one of the mutant plasmid libraries, *E. coli* BL21 (DE3) colonies were picked and used for inoculation of individual pre-cultures in 96-well plates. From each library 73 colonies were selected for a >95% statistical library coverage [12]. Additionally, colonies with the empty vector pETBB (EVC) and the expression vector for wildtype *R_hKICD* (WT) were cultivated as negative control and positive control, respectively. The pre-cultures were cultivated in a polyethylene-sealed 96-well plate with micro-perforations (two holes per well) for gas exchange. Each well contained 200 μL TB and $50 \mu\text{g mL}^{-1}$ kanamycin. After an overnight incubation at 37°C and 190 rpm the $\text{OD}_{600\text{nm}}$ was measured and averaged for all wells. Each pre-culture was used for the inoculation of one well in a 96-deep-well plate containing 1.3 mL TB medium with $50 \mu\text{g mL}^{-1}$ kanamycin. The pre-cultures were then supplemented with 40 μL of 85 % sterile glycerol solution and stored at -80°C . The main cultures were inoculated to a starting $\text{OD}_{600\text{nm}}$ of 0.1 and

subsequently cultivated at 37 °C and 190 rpm for 2.5h until an OD_{600nm} of 0.6-0.8 was reached. Protein production was induced by adding IPTG (final concentration 0.5 mM) to each well, and the cultures were incubated at 25 °C and 250 rpm. for 22 h. Cell growth was determined by measuring at OD_{600nm}. The cells were harvested by centrifuging the plates for 20 min at 2464g, 4 °C (Eppendorf, Centrifuge 5810 R). Next, the supernatant was discarded, and the plate was dried for 10 min. The plate with the cell pellets was sealed with an adhesive aluminum sheet and stored at -80 °C until used for the screening experiment.

For the lysis, the cells in the 96-deep-well plate were thawed on ice. Then 100 µL lysis buffer (10 mM MES, 150 mM NaCl, pH 6.0, B-PER II (Thermo Fisher), 50 U mL⁻¹ Benzonase, 1 mg mL⁻¹ lysozyme and 1 mM phenylmethylsulphonyl fluoride (PMSF) were added to each well. After incubation for 45 min shaking in RT, the cell debris and insoluble protein were pelleted by centrifuging the 96-deep-well plate for 15 min at 2464g and 4 °C. The lysate was kept on ice until the supernatant was used in the subsequent screening assay. For screening of the generated mutant libraries, the DNPH assay was performed as an end-point assay. Thus, the substrate consumption was measured after a predefined time. Before the screening assay, the reaction solutions were prepared with 5 mM of either HPP or KIC substrate and supplemented with cofactors. The screening reactions were started for both substrates in separate 96-well plates by mixing 40 µL cell lysate from each well with 40 µL of the double concentrated reaction solution. In three wells the substrate solution was omitted, and buffer solution without substrate was added instead and used as blank. Hereafter, the two 96-well plates with either HPP or KIC as substrate were incubated at 30 °C for 1h or 3h, respectively. The differential incubation times were chosen due to the lower enzymatic activity of *RnKICD* with the substrate KIC. After the respective time, 25 µL from each well were transferred to a new 96-well plate in which the DNPH assay was conducted as described above. For the analysis of the results, the substrate consumption in the wells with WT or EVC lysate was averaged. The relative substrate consumption rate was determined by calculating the concentration difference, followed by normalization based on the OD₆₀₀ and WT consumption. Potential hits were selected based on two individual criteria: (1) high KIC consumption and (2) altered consumption for one or both substrates. The first selection criterion was chosen to identify mutants with high KIC conversion rates while the second selection criterion was chosen to investigate the effect on the substrate selectivity. The plasmids of the selected hits were then isolated with the GeneJET plasmid mini prep Kit (Thermo Fisher) for Sanger sequencing (Mix2Seq, Eurofins) with a suitable sequencing primer.

In vitro isobutene formation

For in vitro isobutene formation, the reaction mixture (2 mL) consisted of 3 mM KIC substrate solution, 1.2% ethanol (as 250 mM KIC stock solution was prepared in absolute ethanol), 0.5 mM sodium ascorbate, 1 mM dithiothreitol, 0.5 mM FeSO₄, 150 mM NaCl in 10 mM MES buffer pH 6.0. The reaction was initiated by adding purified *RnKICD* wild-type or mutant enzyme (0.1 mg mL⁻¹) to the reaction mixture into 20 mL GC-MS headspace vials (5188-2753, Agilent) sealed with PTFE-lined screw caps (5188-2759, Agilent). The GC-MS vials were incubated at 30 °C for 45 min before isobutene quantification. For WT and F336V *RnKICD*, in vitro isobutene formation was also measured in the presence of competing substrate HPP at concentrations 10 or 1000µM using the same method.

In vivo isobutene formation

For in vivo isobutene production, pre-cultures of *Synechocystis* at OD_{750nm} 0.6 grown in Erlenmeyer flasks were diluted to OD_{750nm} 0.1, then grown to reach OD_{750nm} 0.5-0.6. Then the culture was diluted to OD_{750nm} 0.2 and transferred into 20 mL GC-MS headspace vials (5188-2753, Agilent) filled with 10 mL BG11 medium containing kanamycin (50 µg mL⁻¹), and 50 mM NaHCO₃ (Sigma-Aldrich) was added. The vials were sealed with PTFE-lined screw caps (5188-2759, Agilent), and were shaken horizontally at 120 rpm, under 30 µmol photons m⁻² s⁻¹ at 30 °C. Isobutene was measured after 4 days of incubation from the headspace of the closed vials using GC-MS.

Quantification of isobutene in headspace

Samples from in vitro and in vivo experiments were analyzed by a gas-chromatograph (8890, Agilent), equipped with an HP-1ms Ultra I column (19091S-733UI, Agilent) and an inert mass selective detector (5977B, Agilent). The GC-MS method for the isobutene detection was adopted from Rossoni et al. [23]. Prior to injection, the GC vial was incubated for 5 min at 40 °C to equilibrate isobutene concentration in the vial headspace. For detection and quantification, 100 µL of the headspace was injected at an inlet temperature of 150°C and at a split ratio of 100:1. The oven temperature was set to a constant temperature of 40 °C for 3 min followed by a 2 min temperature increase with 30 °C/min. With this method, the retention time was 1.941 min when an authentic isobutene standard (Air Liquide Gas AB) was analyzed. The MS detector was used in selected ion monitoring (SIM) mode to specifically detect the isobutene typical signals at 41 m/z and 56 m/z. Data analysis was done using OpenChrom [35].) and by comparison with the mass spectra and retention

time of authentic standard. Three replicate injections were performed per sample.

Protein extraction from *Synechocystis*, SDS-PAGE and Western blot

Synechocystis cells were harvested by centrifugation at 4,500 x g for 10 min at 4 °C. The cell pellet was washed in 2 mL phosphate buffered saline (1xPBS), centrifuged and resuspended in 200 µL PBS containing 1 mM PMSF (Merck). Acid-washed glass beads (Sigma-Aldrich) were added, and the cells were disrupted by using a cell homogenizer in three cycles of 30s each (Precellys 24, Bertin Instruments). Protein concentration was determined by DC protein assay (Bio-Rad), using albumin from bovine serum (Sigma-Aldrich) as a standard.

Total cell extract of *Synechocystis* (15 µg crude proteins) was separated on SDS-PAGE gels (Any kD Mini-PROTEAN TGX, Bio-Rad), and blotted to PVDF membrane using the Trans-Blot Turbo system (Bio-Rad). The membrane was rinsed with distilled water and blocked with 20 mL of PBS-T0.1 (0.1% Tween 20) containing 3% bovine serum albumin (BSA) for one hour at room temperature with moderate shaking. Then, the membrane was washed three times with PBS-T0.1 for 5 min followed by a 10 min incubation in 10 mL of PBS-T0.1 containing biotin blocking buffer (IBA Lifesciences). Then, anti-Strep-tag II antibody (Strep-Tactin HRP, IBA Lifesciences) was added, and the membrane was incubated for one hour, followed by two washing steps with 20 mL PBS-T0.1 and twice with 20 mL PBS. Subsequently, Strep-tagged proteins

were detected using the Clarity ECL substrate (Bio-Rad) according to instruction manual, and quantified using Quantity One Software (Bio-Rad).

Statistical analysis

All the data are presented as mean ± standard deviation of three independent biological replications. The statistical analysis was performed by Student's *t*-test, using Excel software (Microsoft). Data were considered significantly different at $p < 0.05$.

Results

Substrate promiscuity of *RnKICD* limits isobutene synthesis

We previously described the recombinant production of α -ketoisocaproate dioxygenase (*RnKICD*) in *Synechocystis* sp. PCC 6803 for the conversion of KIC into isobutene [18]. However, the isobutene synthesis is limited due to the promiscuous activity of *RnKICD*, accepting both KIC and HPP as substrates (Figure 1). Since HPP can act as an inhibitor by competing for the active site for the KIC conversion, we hypothesized that this substrate promiscuity creates a bottleneck for the *in vivo* isobutene biosynthesis. In this work, we applied rational and semi-rational protein engineering on residues in the active site coordination sphere to improve substrate selectivity and thereby *in vivo* isobutene production.

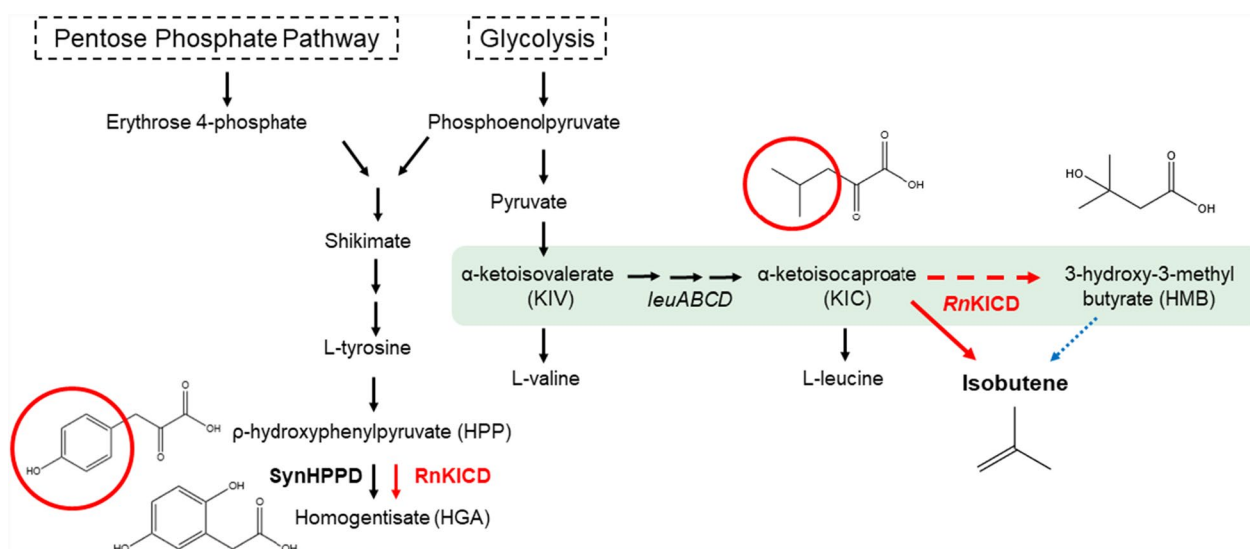


Fig. 1 Involvement of *RnKICD* in the endogenous homogentisate and heterologous isobutene biosynthesis pathways. *RnKICD* utilizes α -ketoisocaproate (KIC) to produce isobutene, and ρ -hydroxyphenylpyruvate (HPP) to produce homogentisate. Black arrows indicate native enzymes; solid and dashed red arrows indicate catalyzed non-native reactions; blue dotted arrow indicates non-enzymatic decomposition. Red circles indicate structural differences between KIC and HPP

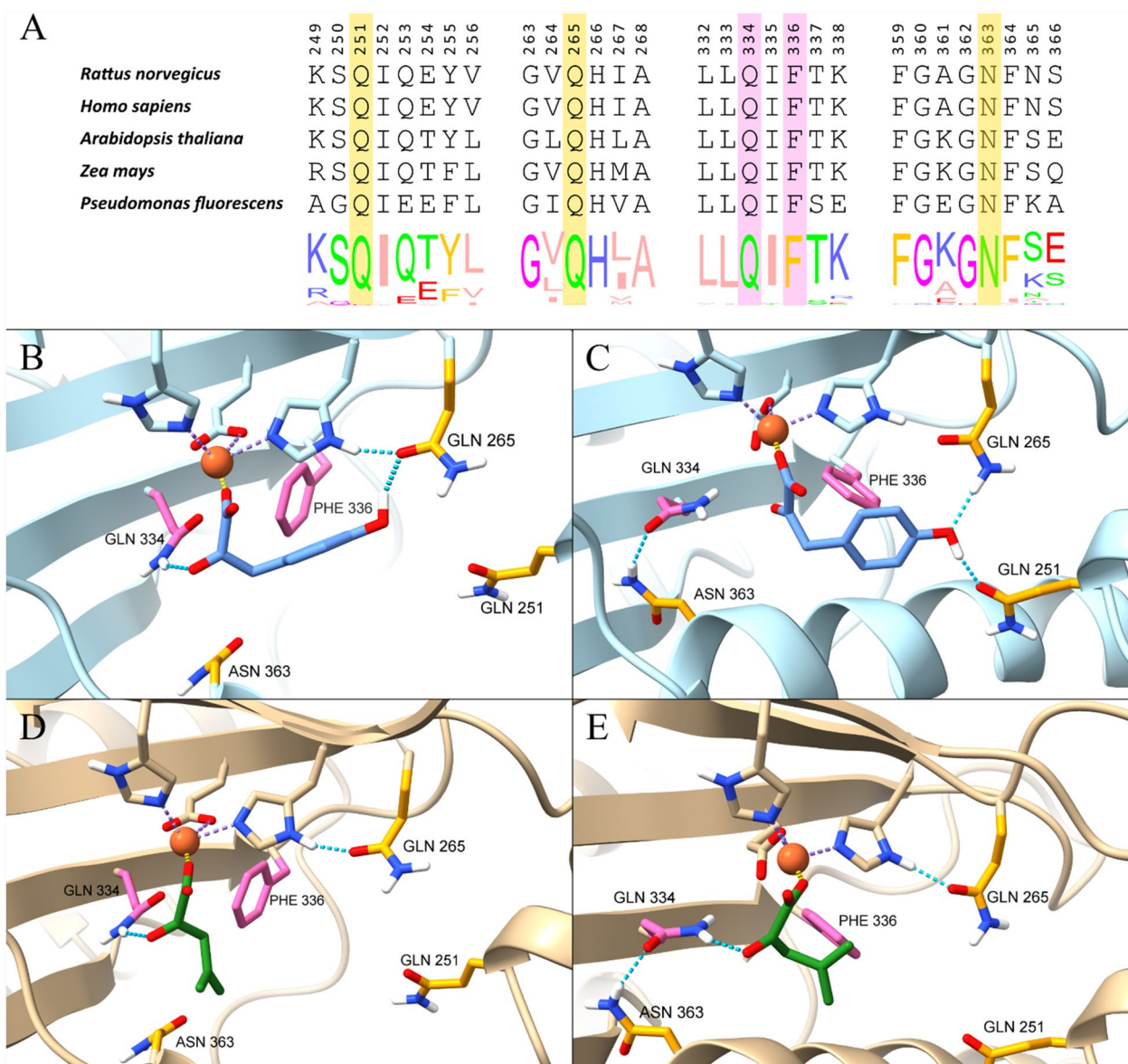


Fig. 2 Sequence and structural analysis of HPPD enzymes. **A.** Alignment of *RnKICD* amino acid sequence with selected sequences of HPPD enzymes from various species and consensus logos showing the conservation within each position. Sections not relevant to this study are omitted for clarity. Normalized consensus logos were generated in Jalview based on the 262 sequences used for multiple sequence alignment. **B.** Homology model of the *RnKICD* active site in open conformation with HPP as substrate. **C.** Homology model of the *RnKICD* active site in closed conformation with HPP as substrate. **D.** Homology model of the *RnKICD* active site in open conformation with KIC as substrate. **E.** Homology model of the *RnKICD* active site in closed conformation with KIC as substrate. Rational design targets are highlighted in yellow, and the site-saturation targets in pink. The structure of HPP is shown in light blue, and the structure of KIC in green. The iron atom is represented by an orange sphere

Selection of amino acid residues in *RnKICD* for protein engineering

The limited mechanistic knowledge of *RnKICD* catalyzing the conversion of KIC represents a challenge for a rational design approach. Yet, the binding of HPP, as well as the catalytic mechanisms of HPPDs (*RnKICD* among them), have been elucidated in several studies [10, 15]. As reported, the main active site residues of HPPD involved

in HPP binding are Q251, Q265, Q334, F336 and N363 (Figure 2A). In the open conformation, the phenolic hydroxyl of HPP forms a hydrogen bond with the side-chain of N363, which helps to direct the substrate into the active site. Then, the substrate flips and the phenol ring instead partakes in hydrogen bonding with Q251 and Q265 as the active site closes. The benzene ring of HPP is also involved in T- π stacking (edge-to-face) with

the phenyl sidechain of F336. Another glutamine residue, Q334, forms a hydrogen bond with the pyruvate moiety of HPP which also interacts with the active site ferrous ion.

To analyze the active site residues of *RnKICD* and its interactions with the substrates HPP and KIC, docking simulations were performed with homology models of *RnKICD* using both open and closed conformations (Figure 2B-E). In docking studies of HPP with homology models of *RnKICD*, similar binding/interactions of HPP with the active site residues were observed as reported in the literature (Figure 2 B-C). In the open conformation, two main binding modes of HPP were observed: 37/50 dockings resulted in hydrogen bonding between HPP and Q265 (Figure 2B) and 13/50 dockings resulted in hydrogen bonding between HPP and N363 (Supplementary Figure 1). Regarding KIC as substrate, we found that KIC is mainly involved in electrostatic interaction with the ferrous ion and hydrogen bonding with Q334 and a probable hydrophobic interaction with F336 (Figure 2D-E).

We targeted F336 for mutagenesis with the hypothesis that substitution of F336 would disrupt the T- π stacking between HPP and F336 and thus reduce the rate of HPP conversion. Furthermore, we targeted Q334 with the aim of reducing formation of the enzyme-HPP complex. Since KIC also interacts with Q334 (Figure 2C-D), it is plausible that the introduction of any mutation at the Q334 position would also effect the interaction with KIC. To find an optimum mutation for F336 and Q334 we used site directed saturation mutagenesis. In addition, we used rational design to examine the effect of the mutations Q251E, Q265E and N363A within the active site. We hypothesized that the replacement of glutamine with glutamate (Q251E and Q265E) would introduce an electrostatic repulsion effect towards HPP, while retaining a

similar structural composition of the active site. The substitution of asparagine with an alanine at position 363 would decrease HPP binding due to disruption of hydrogen bonding and might also result in favored KIC binding, due to an increased hydrophobic interaction.

Screening of site-saturation mutant libraries

To evaluate the expected nucleobase distribution of the site-saturation libraries, a quick quality control (QQC) sequencing protocol was used, targeting the codons for Q334 and F336 [12]. The QQC matched in both cases qualitatively the expected nucleobase distribution with exclusively T or G in the third codon position, while including all four nucleobases in the first and second position (Supplementary Figure 2). Recombinantly-produced *RnKICD* variants were thereafter screened for altered substrate selectivity compared to wild type (WT) enzyme. Hits from both libraries were selected based on (I) high KIC consumption activity and (II) altered substrate consumption for one or both substrates (Figure 3). Additionally, sequencing was performed and translated amino acids in each variant were identified.

All selected variants with wildtype-like high KIC consumption (criterion I) were found to be expressing non-altered *RnKICD* variants, highlighting the importance of Q334 and F336 for high consumption of KIC. From the Q334 mutant library, five mutants were selected based on criterion II, showing WT *RnKICD*-like HPP consumption but disrupted KIC consumption. These results suggest that mutations Q334S and Q334T contributed to increased HPP selectivity, reinforcing the importance of Q334 in KIC consumption by *RnKICD* (Figure 3A). The EVC control showed overall no HPP consumption indicating the absence of a HPPD enzyme when *RnKICD* is not expressed. Two F336 library mutants displayed

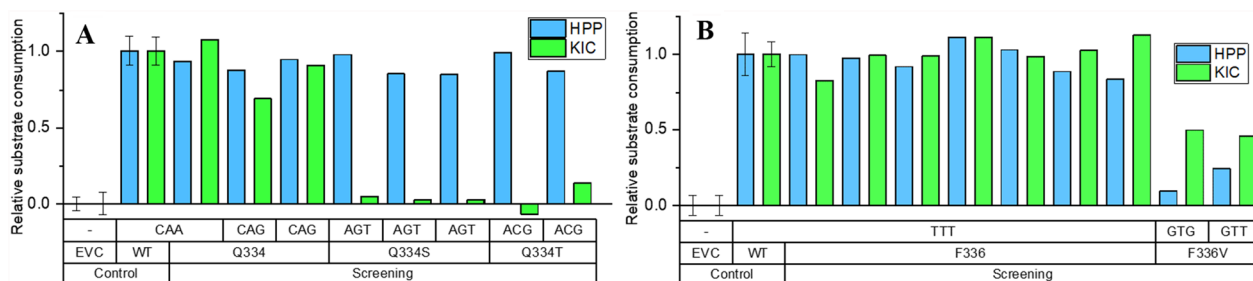


Fig. 3 Selected hits from the lysate activity screens of *E. coli* transformant libraries generated by site-saturation mutagenesis. Potential hits for the F336 and Q334 libraries were selected based on two individual criteria: (I) high KIC consumption and (II) altered consumption for one or both substrates. **A.** Screening result for the selected colonies from the Q334X mutant library. Relative consumption rate of KIC (green) and HPP (blue) by Q334X mutants in comparison to WT with the introduced codon and translated amino acid below. Relative consumption rate with respect to the WT (set to 1.0) was calculated by normalizing the consumption over time based on OD_{600} . **B.** Screening result for the selected colonies from the F336X mutant library. Relative consumption rate of HPP (blue) and KIC (light green) by F336X mutants in comparison to WT with the introduced mutation below. WT and empty vector control (EVC) for comparison are shown as average with a standard deviation from eight wells per 96-well plate

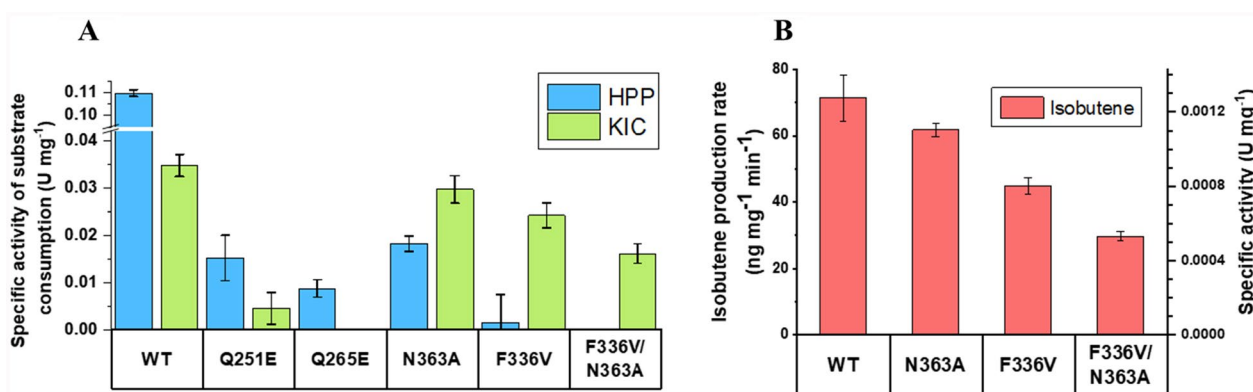


Fig. 4 Functional characterization of *RnKICD* variants. **A.** Initial KIC and HPP consumption rate at 2.5 mM substrate expressed as specific activity (U mg^{-1}) calculated based on the consumption activity in μmol of substrate. The rates were calculated based on the slope (substrate amount vs. time, see Supplementary Figure 5) as technical triplicates and corrected by the non-enzymatic degradation of the substrate (negative control). **B.** Isobutene production rate ($\text{ng mg}^{-1} \text{min}^{-1}$) (right y-axes), and specific activity (U mg^{-1} with $\text{U} = \mu\text{mol min}^{-1}$) (left y-axes, was measured in an end point assay after 45 min using GC-MS. The measurements were taken as technical triplicates with 3 mM KIC in the reaction

altered substrate consumption (criterion II), with mutation F336V enhancing selectivity towards KIC. In this mutant, HPP consumption was reduced about 7-fold compared to WT, while KIC consumption decreased only 2-fold (Figure 3B). The slight reduction in KIC consumption was considered a side effect of the mutation.

In vitro analysis of *RnKICD* and generated variants

The previously mentioned rationally designed variants (Q251E, Q265E and N363A) and the best performing variant from the semi-rational design (F336V) were purified (Supplementary Figure 3) and assessed with regards to consumption of substrates KIC and HPP, as well as formation of isobutene (Figure 4). We found that the mutations Q251E and Q265E resulted in *RnKICD* variants with significantly reduced activity. Both mutations decreased HPP consumption by approximately 10-fold while the KIC consumption was too small to measure. (Figure 4A). Consequently, the *in vitro* measurements for these variants resulted in no detectable isobutene formation (data not shown). In contrast, N363A had comparable KIC consumption rate and isobutene formation to that of WT *RnKICD*, while the HPP consumption was ~10-fold lower (Figure 4A-B). Hence, the selectivity towards KIC was enhanced by the N363A amino acid substitution. For F336V, the consumption rate of HPP was critically impaired, while the KIC consumption and isobutene production rates were 35% and 40% lower as compared to WT, respectively (Figure 4A-B).

The two single-point mutations that retained KIC consumption activity (F336V, N363A) resulted in different characteristics compared to WT *RnKICD*. N363A exhibited an improved selectivity towards KIC with retained

isobutene production, while F336V showed even higher selectivity, but with decreased KIC consumption and isobutene production *in vitro*. In order to explore any synergistic effects between the two mutations, the double mutant F336V/N363A was created. This new variant displayed a complete disruption of the HPP consumption whereas the KIC consumption and isobutene production were both retained at lower levels, as compared to the single-point mutations. Yet, comparing the specific activities of isobutene formation and KIC consumption revealed that all three variants exhibited similar KIC-to-isobutene conversion ratios (3.3–3.7%), comparable to the wild type (Supplementary Table 3). This observation is a strong indication that the conversion of KIC is catalytically promiscuous in which only a small fraction of the consumed KIC forms isobutene. Additionally, the *in vitro* isobutene production was hindered by the presence of competing substrate HPP in both the WT and F336V mutant variants (Supplementary Figure 4).

In vivo analysis of engineered *Synechocystis* strains

The results obtained by the *in vitro* assays revealed a higher substrate specificity for some of the *RnKICD* variants, leading to a potential for improving isobutene production *in vivo*. Therefore, the genes encoding WT *RnKICD* and the best performing mutant variants were individually introduced into *Synechocystis*, resulting in the strains Syn-KICD, Syn-N363A, Syn-F336V and Syn-F336V/N363A, respectively (Table 1). The performance of *Synechocystis* strains producing the different *RnKICD* variants was evaluated in terms of growth and final isobutene titer (Figure 5). No significant growth differences were observed among the examined *Synechocystis* strains (Figure 5A), indicating that, although the

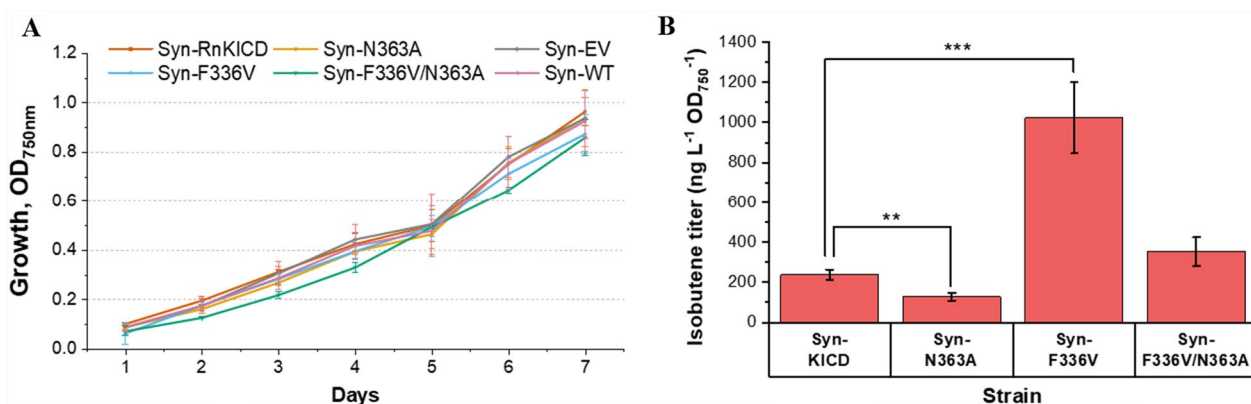


Fig. 5 Production capabilities of *Synechocystis* strains overexpressing *RnKICD* and its variants after four days of batch cultivation. **A.** Growth of isobutene-producing strains, as indicated by optical density (OD_{750nm}). **B.** Isobutene production titer (ng L⁻¹ OD_{750nm}⁻¹) normalized to the culture density (OD_{750nm}). All the results represent the mean of five biological replicates; error bars represent the standard deviation. Asterisks represent significant differences between the corresponding strain and the base strain, ** p < 0.01, *** p < 0.001 in *t*-test

production of *RnKICD* impose a burden to the cell both in terms of protein cost and redirection of carbon flux, cell growth did not appear to be affected. After four days of batch cultivation in GC-MS vials (Figure 5B), strains Syn-KICD and Syn-F336V/N363A showed a comparable isobutene production, while the isobutene production by Syn-N363A was decreased significantly. However, Syn-F336V exhibited a considerable increase, comprising a 4-fold enhancement of absolute isobutene titers as well as growth-related titers, as compared to the base strain (Syn-KICD) (Figure 5B and Supplementary Figure 6).

Discussion

In this study, semi-rational protein engineering of *RnKICD* has been employed to enhance substrate specificity towards α -ketoisocaproate (KIC) in vitro and isobutene production titers in vivo. We identified two *RnKICD* variants F336V and F336V/N363A that exhibited an improvement in substrate selectivity, of which F336V resulted in higher isobutene production in *Synechocystis*.

As previously shown by crystallographic and spectroscopic studies [10], the active site of HPPD is enclosed by a C-terminal α -helix, exhibiting two distinct orientations, assuming to function as a gate that controls the binding of the substrate in the active site [16]. This helix is either in a closed conformation, shielding the active site from the solvent, or in an open conformation that allows access of substrate to the binding pocket. The catalysis is initiated by a bidentate interaction of HPP with the ferrous ion in the active site, hydrogen bonds with a conserved glutamine residue (Q334) and an association with the molecular oxygen, resulting in an octahedral coordination geometry involving a facial triad (H183, H266 and E349). This is followed by a keto acid moiety

decarboxylation, phenyl ring hydroxylation, and side-chain re-arrangement.

Rational and semi-rational protein design for identifying amino acids substitutions linked to altered substrate selectivity of *RnKICD*

Earlier studies show that by replacing the glutamines Q251 and Q265 to a glutamate in the active site of HPPD, the ability to form hydrogen bonds with the hydroxyl group of HPP was lost, thus decreasing the stability of the enzyme-substrate complex [22]. Therefore, we initially reasoned that introducing Q251E and Q265E mutations would reduce competition with KIC binding. However, our results indicate that these mutations not only impacted the HPP consumption, but also diminished KIC consumption. This highlights the importance of these glutamines for the structural integrity of the active site in *RnKICD*. For future studies, substituting Q265 with smaller polar amino acids, such as serine or threonine might be a strategy to decrease the binding affinity of HPP whilst preserving the hydrogen bond with iron ligating residue H266.

The residue N363 is thought to play a role in the rotation of the C-terminal helix hinge region [10], which helps to bind HPP to the active site in its open conformation (Supplementary Figure 1). Previous studies demonstrated that the mutation N363A decreased k_{cat}/K_m for HPP by 5-fold compared to the WT enzyme [10]. Under our in vitro assay conditions, N363A showed similarly a 6-fold decrease in HPP consumption, while the KIC consumption was not affected. This change likely results from the decreased stabilization of HPP in the open conformation of *RnKICD*. However, in vivo studies revealed that the Syn-N363A strain produced about

half the amount of isobutene, compared to the Syn-KICD strain. These findings suggest that while the N363A substitution significantly reduced HPP consumption in vitro, HPP may still be able to interact with the active site due to alternative binding (Figure 2B). Thus, HPP could compete with KIC binding at the active site and thereby impact the isobutene production in *Synechocystis*.

In our semi-rational design library screening of F336X and Q334X, we aimed to identify hits with altered selectivity towards one of the two substrates. We got two hits with increased selectivity towards HPP, Q334S and Q334T (Figure 3B). The loss of KIC activity in these mutants could be explained by the docking simulations on the *RnKICD* homology model, showing that Q334 is probably essential for the KIC turnover, since it is the only amino acid directly interacting with KIC as substrate in both the open and closed conformations (Figure 2D-E).

Regarding the F336X variants, the absence of T- π stacking against the phenyl sidechain of F336 resulted in reduced activity towards HPP, whereas the activity towards KIC was not compromised to the same extent. This indicated that F336V is a promising candidate for improved isobutene production in vivo. Earlier kinetic experiments on HPPD showed that F336 does not directly participate in the catalysis of HPPD, but has importance for stabilizing the HPP-enzyme complex [22]. The replacement of F336 with nonpolar amino acids, such as valine, could increase interaction of KIC. It might be that alanine is too small to sustain substrate stabilization, whereas larger apolar amino acids, such as valine, seem to be beneficial for the formation of the enzyme-substrate complex. As the obtained in vitro isobutene formation rates were low in comparison to KIC consumption rates, it can be concluded that *RnKICD* is catalytically promiscuous and isobutene is only formed as by-product, as previously discussed [18]. We also observed that the presence of HPP inhibited the isobutene production in both the F336V and WT versions in a similar manner. Hence the mutation did not appear to affect the competition at the active site of *RnKICD*.

Targeting *RnKICD* substrate selectivity yields optimized biosynthetic pathway for isobutene production

This study aimed to enhance *RnKICD* selectivity for KIC as isobutene precursor using rational and semi-rational protein design. The optimized enzymes were assessed in vitro for their substrate consumption profiles, and strains exhibiting a preference for KIC over HPP, were tested in vivo to strategically redirect biosynthesis toward increased isobutene production in

Synechocystis. The goal was successfully achieved, as strains Syn-F336V and Syn-F336V/N363A demonstrated improved isobutene production, with Syn-F336V producing a four-fold higher isobutene titer compared to base strain. However, the in vitro KIC to isobutene conversion was not apparently enhanced in any of the mutant versions of *RnKICD*.

In *Synechocystis*, *RnKICD* acts in two distinct metabolic pathways resulting in a competition between KIC and HPP for the active site. Consequently, a decreased affinity for HPP also reduces the inhibition of the KIC-to-isobutene conversion. Besides, the catalyzed reaction may be influenced by the cellular environment, including factors such as substrate concentrations and pH levels.

The divergent isobutene production rates by F336V and WT in vitro and in vivo suggest that environmental factors unique to the cellular context have a major influence on the enzymatic activity. The in vitro assays do not account for cellular factors such as the native HPP consumption by *SynHPPD* or native co-substrates that help to reduce the mononuclear iron in the active site after one catalytic cycle. *RnKICD* is using both KIC and oxygen as substrates, thus the *RnKICD* activity might be limited by oxygen and KIC concentration under in vitro and in vivo conditions, respectively. The oxygen-rich cellular environment of cyanobacteria could enhance the catalysis of the enzyme and thus explain at least part of the differential rates of isobutene production detected in vitro and in vivo.

Conclusions

Using a semi-rational design, we first created an *RnKICD* mutant library that was screened for enzyme variants with improved KIC-to-HPP consumption ratio and thus with a potential of increased in vivo isobutene formation. These enzymes were purified and characterized for improved isobutene formation. Different *RnKICD* variants exhibited increased preference towards KIC as substrate and isobutene as product. Q251 and Q265 were found to be essential in retaining activity of *RnKICD* independent of substrate. The introduced mutations in position Q334 disrupted the activity towards KIC, suggesting a distinct role of Q334 for KIC to isobutene formation. Further, we suggest that F336 and N363 are important for modulating selectivity between the two substrates HPP and KIC. Mutant strains of *Synechocystis* carrying the F336V variant increased isobutene production in vivo. The enhanced production of isobutene in the F336V strain underlines the importance of taking the in vivo context in consideration in designing in vitro enzymatic assays as a tool for enhanced metabolite production. We conclude that

a strategy of rational design and site-specific saturation mutagenesis within the active site of *RnKICD* is a potent strategy for increasing substrate specificity and thus redirecting metabolic fluxes for improved isobutene bioproduction in *Synechocystis*.

Supplementary Information

The online version contains supplementary material available at <https://doi.org/10.1186/s12934-025-02708-x>.

Additional file 1.

Acknowledgements

This work was supported by FORMAS—A Swedish Research Council for Sustainable Development (Project No. 2021-01669), the Swedish Energy Agency (Project No. 44728-1) and the European Union Horizon Europe – the Framework Program for Research and Innovation (2021–2027) under the grant agreement number 101070948 (Project PhotoSynH2).

Author contributions

CS: Methodology, Investigation, Formal analysis, Validation, Visualization, Writing-Review & Editing. AK: Methodology, Investigation, Formal analysis, Validation, Visualization, Writing-Original Draft, Writing-Review & Editing. BS: Investigation, Formal analysis, Validation, Writing-Review & Editing. GS: Supervision, Funding Acquisition. HL: Supervision, Visualization, Writing-Review & Editing. CB: Supervision, Writing-Review & Editing. KS: Conceptualization, Supervision, Funding Acquisition, Writing-Review & Editing.

Funding

Open access funding provided by Uppsala University.

Availability of data and materials

No datasets were generated or analysed during the current study.

Declarations

Competing interests

The authors declare no competing interests.

Author details

¹Department of Chemistry-Ångström Laboratory, Uppsala University, 751 20 Uppsala, Sweden.

Received: 29 December 2024 Accepted: 31 March 2025

Published online: 23 April 2025

References

- Baldwin JE, Crouch NP, Fujishima Y, Lee MH, MacKinnon CH, Pitt JPN, Willis AC. 4-hydroxyphenylpyruvate dioxygenase appears to display α -ketoisocaproate dioxygenase activity in rat liver. *Bioorg Med Chem Lett*. 1995;5:1255–60.
- Bilal M, Iqbal HMN, Guo S, Hu H, Wang W, Zhang X. State-of-the-art protein engineering approaches using biological macromolecules: a review from immobilization to implementation viewpoint. *Int J Biol Macromol*. 2018;108:893–901.
- Case DA, Aktulga HM, Belfon K, Cerutti DS, Cisneros GA, Cruzeiro VWD, Forouzes N, Giese TJ, Götz AW, Gohlke H, Izadi S, Kasavajhala K, Kaymak MC, King E, Kurtzman T, Lee TS, Li P, Liu J, Luchko T, Luo R, Manathunga M, Machado MR, Nguyen HM, O'Hearn KA, Onufriev AV, Pan F, Pantano S, Qi R, Rahnamoun A, Rishch A, Schott-Verdugo S, Shajan A, Swails J, Wang J, Wei H, Wu X, Wu Y, Zhang S, Zhao S, Zhu Q, Cheatham TE 3rd, Roe DR, Roitberg A, Simmerling C, York DM, Nagan MC, Merz KM Jr. AmberTools. *J Chem Inform Model*. 2023;63:6183–91.
- Crouch NP, Adlington RM, Baldwin JE, Lee M-H, MacKinnon CH. A mechanistic rationalisation for the substrate specificity of recombinant mammalian 4-hydroxyphenylpyruvate dioxygenase (4-HPPD). *Tetrahedron*. 1997;53:6993–7010.
- Fukuda H, Fujii T, Sukita E, Tazaki M, Nagahama S, Ogawa T. Reconstitution of the isobutene-forming reaction catalyzed by cytochrome P450 and P450 reductase from *Rhodotorula minuta*: decarboxylation with the formation of isobutene. *Biochem Biophys Res Commun*. 1994;201:516–22.
- Gasteiger E, Hoogland C, Gattiker A, Duvaud SE, Wilkins MR, Appel RD, Bairoch A. Protein identification and analysis tools on the ExPASy server. In: *The proteomics protocols handbook*. 2005:571–607.
- Gogerty DS, Bobik TA. Formation of isobutene from 3-hydroxy-3-methylbutyrate by diphosphomevalonate decarboxylase. *Appl Environ Microbiol*. 2010;76:8004–10.
- Gholami Z, Gholami F, Tišler Z, Vakili M. A review on the production of light olefins using steam cracking of hydrocarbons. *Energies*. 2021;14:8190.
- Gong L, Xu G, Cao X, Han R, Dong J, Ni Y. High-throughput screening method for directed evolution and characterization of aldol activity of D-Threine aldolase. *Appl Biochem Biotechnol*. 2021;193:417–29.
- Huang CW, Hwang CC, Chang YL, Liu JT, Wu SP, Huang KL, Huang W, Lee HJ. Functional role of residues involved in substrate binding of human 4-hydroxyphenylpyruvate dioxygenase. *Biochem J*. 2021;478:2201–15.
- Jamil OK, Cravens A, Payne JT, Kim CY, Smolke CD. Biosynthesis of tetrahydrodropaverine and semisynthesis of papaverine in yeast. *Proc Natl Acad Sci*. 2022;119: e2205848119.
- Kille S, Acevedo-Rocha CG, Parra LP, Zhang ZG, Opperman DJ, Reetz MT, Acevedo JP. Reducing codon redundancy and screening effort of combinatorial protein libraries created by saturation mutagenesis. *ACS Synth Biol*. 2013;2:83–92.
- Krieger E, Vriend G. YASARA View—molecular graphics for all devices—from smartphones to workstations. *Bioinformatics*. 2014;30:2981–2.
- Land H, Humble MS. YASARA: a tool to obtain structural guidance in biocatalytic investigations. In: *Methods in molecular biology*. Humana Press. 2018. pp. 43–67.
- Lin HY, Chen X, Chen JN, Wang DW, Wu FX, Lin SY, Zhan CG, Wu JW, Yang WC, Yang GF. Crystal structure of 4-hydroxyphenylpyruvate dioxygenase in complex with substrate reveals a new starting point for herbicide discovery. *Research*. 2019;2019:2602414.
- Lin JF, Sheih YL, Chang TC, Chang NY, Chang CW, Shen CP, Lee HJ. The interactions in the carboxyl terminus of human 4-hydroxyphenylpyruvate dioxygenase are critical to mediate the conformation of the final helix and the tail to shield the active site for catalysis. *PLoS ONE*. 2013;8(10): e69733.
- Marchionna M, Di Girolamo M, Patrini R. Light olefins dimerization to high quality gasoline components. *Catal Today*. 2001;65(2–4):397–403.
- Mustila H, Kugler A, Stensjö K. Isobutene production in *Synechocystis* sp. PCC 6803 by introducing α -ketoisocaproate dioxygenase from *Rattus norvegicus*. *Metab Eng Commun*. 2021;12:e00163.
- Nicholas CP. Applications of light olefin oligomerization to the production of fuels and chemicals. *Appl Catal A Gen*. 2017;543:82–97.
- Norris SR, Barrette TR, DellaPenna D. Genetic dissection of carotenoid synthesis in *Arabidopsis* defines plastocyanin as an essential component of phytoene desaturation. *Plant Cell*. 1995;7:2139–49.
- Ochman H, Gerber AS, Hartl DL. Genetic applications of an inverse polymerase chain reaction. *Genetics*. 1988;120:621–3.
- Raspail C, Graindorge M, Moreau Y, Crouzy S, Lefebvre B, Robin AY, Dumas R, Matringe M. 4-hydroxyphenylpyruvate dioxygenase catalysis: Identification of catalytic residues and production of a hydroxylated intermediate shared with a structurally unrelated enzyme. *J Biol Chem*. 2011;286:26061–70.
- Rossoni L, Hall SJ, Eastham G, Licence P, Stephens G. The putative mevalonate diphosphate decarboxylase from *Picrophilus torridus* is in reality a mevalonate-3-kinase with high potential for bioproduction of isobutene. *Appl Environ Microbiol*. 2015;81:2625–34.
- Saaret A, Villiers B, Stricher F, Anissimova M, Cadillon M, Spiess R, Hay S, Leys D. Directed evolution of prenylated FMN-dependent Fdc supports efficient *in vivo* isobutene production. *Nat Commun*. 2021;12:5300.
- Sabourin PJ, Bieber LL. The mechanism of alpha-ketoisocaproate oxygenase. Formation of beta-hydroxyisovalerate from alpha-ketoisocaproate. *J Biol Chem*. 1982;257(13):7468–71.

26. Sabourin PJ, Bieber LL. Formation of β -hydroxyisovalerate by an α -ketoisocaproate oxygenase in human liver. *Metabolism*. 1983;32:160–4.
27. Shenoy AR, Visweswariah SS. Site-directed mutagenesis using a single mutagenic oligonucleotide and DpnI digestion of template DNA. *Anal Biochem*. 2003;319:335–6.
28. Sievers F, Wilm A, Dineen D, Gibson TJ, Karplus K, Li W, Lopez R, McWilliam H, Remmert M, Söding J, Thompson JD, Higgins DG. Fast, scalable generation of high-quality protein multiple sequence alignments using Clustal Omega. *Mol Syst Biol*. 2011;7:539.
29. Stanier RY, Kunisawa R, Mandel M, Cohen-Bazire G. Purification and properties of unicellular blue-green algae (order Chroococcales). *Bacteriol Rev*. 1971;35:171–205.
30. Tcvetkov P, Cherepovitsyn A, Fedoseev S. The changing role of CO₂ in the transition to a circular economy: review of carbon sequestration projects. *Sustainability*. 2019;11(20):5834.
31. Trautmann D, Voss B, Wilde A, Al-Babili S, Hess WR. Microevolution in cyanobacteria: re-sequencing a motile substrain of *Synechocystis* sp. PCC 6803. *DNA Res*. 2012;19:435–48.
32. van Leeuwen BNM, van der Wulp AM, Duijnsteer I, van Maris AJA, Straathof AJJ. Fermentative production of isobutene. *Appl Microbiol Biotechnol*. 2012;93:1377–87.
33. Wang DW, Lin HY, Cao RJ, Chen T, Wu FX, Hao GF, Chen Q, Yang WC, Yang GF. Synthesis and herbicidal activity of triketone-quinoline hybrids as novel 4-hydroxyphenylpyruvate dioxygenase inhibitors. *J Agric Food Chem*. 2015;17:5587–96.
34. Wells JA, Vasser M, Powers DB. Cassette mutagenesis: an efficient method for generation of multiple mutations at defined sites. *Gene*. 1985;34:315–23.
35. Wenig P, Odermatt J. OpenChrom: a cross-platform open source software for the mass spectrometric analysis of chromatographic data. *BMC Bioinformatics*. 2010;11:405.
36. Xiong W, Liu B, Shen Y, Jing K, Savage TR. Protein engineering design from directed evolution to de novo synthesis. *Biochem Eng J*. 2021;174:108096.
37. Zheng L, Baumann U, Reymond JL. An efficient one-step site-directed and site-saturation mutagenesis protocol. *Nucleic Acids Res*. 2004;32:e115.

Publisher's Note

Springer Nature remains neutral with regard to jurisdictional claims in published maps and institutional affiliations.